

LOW-TEMPERATURE PLASMAS

Effect of the Magnetic-Field Configuration on the Plasma Parameters in a Microwave ECR Discharge

N. P. Poluektov, Yu. P. Tsar'gorodsev, and I. G. Usatov

Department of Physics, Moscow State University of Forestry,
Pervaya Institutskaya ul. 1, Mytishchi, Moscow oblast, 141005 Russia

Received September 23, 1998; in final form, January 21, 1999

Abstract—Results are presented from studies of a plasma in a microwave ECR discharge for different magnetic-field configurations.

1. INTRODUCTION

In connection with the production of microelectronic components of submicron size, considerable attention is being given to devices based on microwave electron-cyclotron resonance (ECR) discharges [1–3]. In these devices, the plasma is produced in a magnetic field due to the efficient ECR absorption of microwave energy. This makes it possible to produce a plasma at pressures of 0.01 to 5 mtorr with a density higher than 10^{11} cm⁻³ and a degree of ionization of 1 to 10%. Among other advantages of these devices, we mention the following: the absence of an incandescent cathode allows one to work with reactive gases; the neutral and ion temperatures are rather low (<1 eV); and the energy of ions arriving at a substrate is about tens of eV and can be easily controlled, thereby providing necessary conditions for anisotropic etching of submicron structures. Microwave ECR discharges are employed for the production of thin films by sputtering of metal targets;

deposition of dielectric (including diamond) films; and etching of submicron (down to 0.15 μm) features on Si, SiO₂, GaAs, AlGaAs, InP, and other films. Experiments showed that the most important parameters of an ECR plasma that govern the technological characteristics of this class of device depend substantially on the configuration of the magnetic field. At present, plasma sources with different magnetic-field configurations are being investigated, namely, a solenoidal configuration produced by electromagnets or a cusp configuration produced by permanent magnets. In this paper, we present the results of experiments carried out in a device in which the magnetic field is a combination of solenoidal and cusp fields.

2. EXPERIMENTAL APPARATUS

A detailed description of the device is presented in [4], and its schematic is shown in Fig. 1. The vacuum

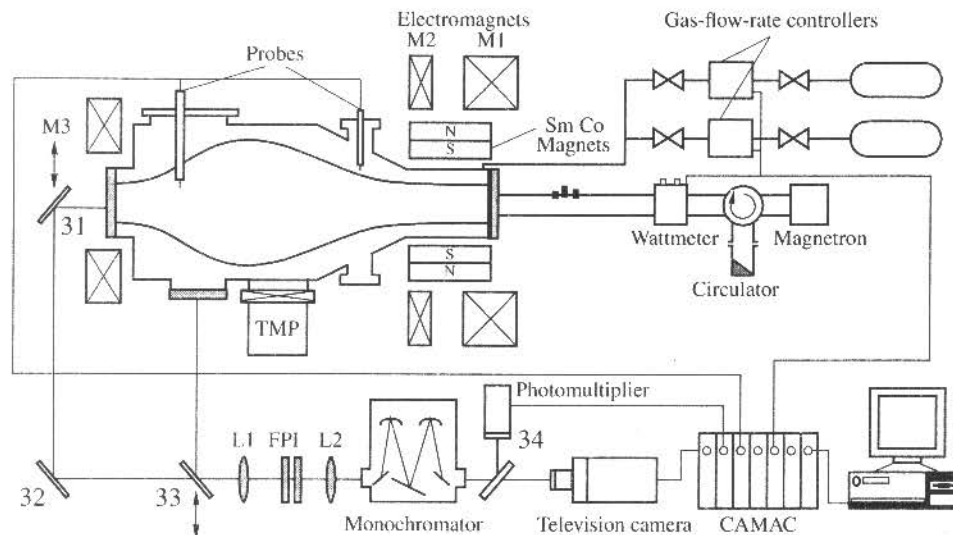


Fig. 1. Schematic of the device.

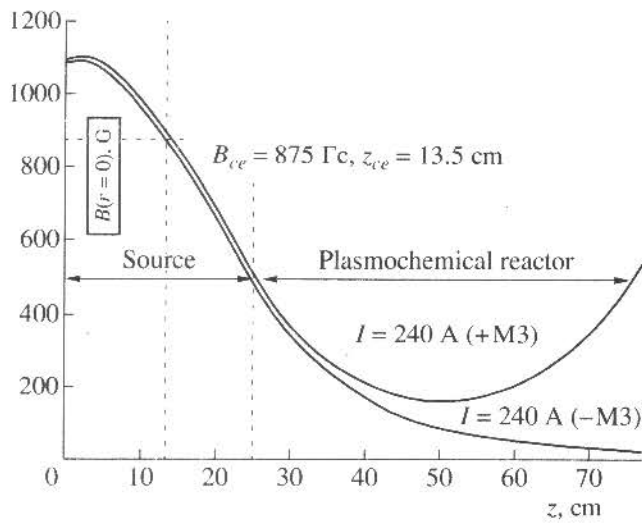


Fig. 2. Longitudinal profiles of the magnetic field produced by the electromagnets at $r = 0$ for $I_{el.m} = 240$ A.

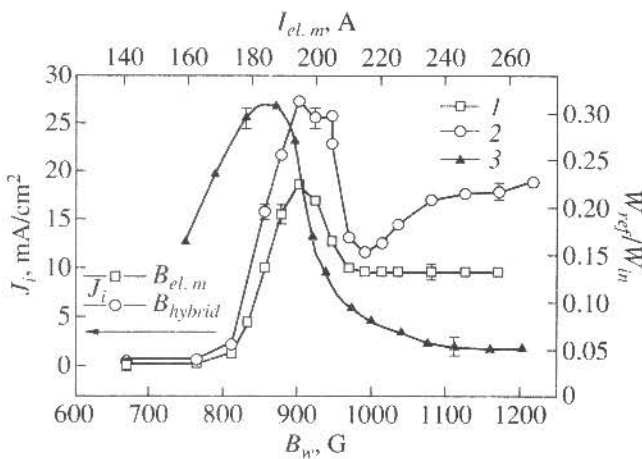


Fig. 3. Ion current density J_i in (1) the magnetic field produced by electromagnets $B_{el.m}$ and (2) hybrid magnetic field and (3) the ratio between the reflected and incident microwave powers, W_{ref}/W_{in} , as functions of the magnetic field; Kr, $p = 0.6$ mtorr, the flow rate is 10 secm, $W = 900$ W, $r = 0$, and the distance from the input window is $z = 62$ cm.

chamber consists of a plasma source (15 cm in diameter and 25 cm long) and plasmochemical reactor (35 cm in diameter and 60 cm long). A vacuum (10^{-6} torr) is produced by turbomolecular pumps (TMPs). The working gas is injected into the chamber through a mass flow controller located near a quartz window. Microwaves at a frequency of 2.45 GHz are generated by a magnetron of 1-kW power, transmitted by a 90×45 mm waveguide, and launched into the discharge chamber through a quartz window. Transmitted and reflected powers are measured by a wattmeter. The magnetic field is created by three electromagnets and 12 perma-

nent SmCo magnets. The magnet M3 can be either switched on or switched off, and the solenoidal field of the electromagnets can be varied by changing the magnet position. Figure 2 shows the magnetic field on the device axis for a current of 240 A. The field in the source is radially uniform (accurate to 4%) within a region 15 cm in diameter. Twelve permanent magnets $15 \times 20 \times 120$ mm in size with alternate poles are positioned around the source. They create a cusp magnetic field with a magnitude of 875 G at a distance of 1 cm from the wall.

All measurements were conducted with the help of CAMAC modules and an IBM computer. The plasma density, the floating and plasma potentials, the electron temperature, and the electron energy distribution function (EEDF) were measured by Langmuir probes (0.35 mm in diameter and 5–10 mm long), oriented perpendicularly to the magnetic field. The current–voltage characteristic of each probe was measured for 20–30 s. A program for processing the current–voltage characteristics (with built-in graphics options) smoothed the data with splines and calculated the first and second derivatives. The plasma density was calculated from the ion saturation current (at a probe voltage of 80 V) with account of the change in the effective probe surface area [5]. The electron temperature was found from the slope of the logarithm of the first derivative of the current with respect to the voltage. The EEDF was assumed to be proportional to the second derivative, and the plasma potential was determined by the zero of the second derivative. The temperature of atoms and ions (Ar, Kr, and Xe) was found from spectroscopic measurements with a Fabry–Perot interferometer (the schematic of measurements is shown in Fig. 1). To record interferograms, we used a television camera consisting of a highly sensitive LI-702 vidicon with an installed image converter. Signals from the camera were digitized with an ADC CAMAC module, which recorded a $256 \times 256 \times 8$ -bit frame for 20 ms. The buffer memory could store four frames. For low-intensity spectral lines, data were averaged over 128 frames.

Spectra of plasma emission from various plasma regions were measured with an MDR-12 monochromator and a photomultiplier. Photomultiplier signals were fed to an F4225 ADC (10 bit, 1 MHz, 128-kByte buffer memory), which allowed us to record the emission spectrum in the range from 200 to 800 nm for 5 min.

3. RESULTS AND THEIR DISCUSSION

3.1. Discharge in a Solenoidal Field

In this series of experiments, we studied the production of a plasma at pressures of 0.1 to 2 mtorr in a solenoidal magnetic field created by electromagnets only. In Fig. 3, squares show the ion saturation current density J_i in a Kr plasma on the device axis as a function of the magnetic field. The B_w values correspond to the inner surface of the input quartz window, where the

field is maximum. As the field increases from 850 to 900 G, the ion current density and, consequently, the plasma density increase sharply. This shows that the ECR conditions are satisfied; for the frequency $f = 2.45$ GHz, this corresponds to the field $B_{ce} = 875$ G. Note that the resonant increase in the plasma density begins at fields somewhat lower than B_{ce} . This is explained by the Doppler broadening of the resonance. Let us estimate the spread in the resonant field values.

(i) First, we take into account the effect of a finite width of the generator emission line. For an M-105 magnetron, the FWHM of the emission spectrum, measured with an ISPM-1 spectrometer, is equal to $\Delta\omega_G \approx 20$ MHz. Thus, we obtain

$$\frac{\Delta\omega_G}{\omega_G} \approx \frac{\Delta B_{ce}}{B_{ce}} \approx 0.8 \times 10^{-2}.$$

(ii) Now we consider the effect of electron thermal motion. For typical values of the electron thermal velocity $V_{Te} = 1.3 \times 10^6$ m/c and plasma refractive index

$$n = 5 \text{ [6]}, \text{ we have } \frac{\Delta B_{ce}}{B_{ce}} \approx 2 \frac{n}{c} V_{Te} \approx 4.3 \times 10^{-2}, B_{ce 1-2} =$$

$\frac{m_e c}{e} (\omega \mp k V_{Te})$, where m_e is the electron mass, c is the speed of light, k is the wavenumber, and $\omega = 2\pi f$. It is seen that the Doppler effect related to electron thermal motion prevails and the width of the interval of resonant magnetic fields is $\Delta B_{ce} \approx 4.3 \times 10^{-2} B_{ce} \approx 40$ G, which agrees with that observed in the experiment.

The maximum ion current density (18 mA/cm²) for a microwave power of $W = 900$ W is attained for $B_w \approx 900$ G. This corresponds to the density $N = 5 \times 10^{11}$ cm⁻³, which substantially exceeds the critical density ($N_{cr} = 7.4 \times 10^{10}$ cm⁻³ [7]). In addition to the high density, we observed a strong radial nonuniformity of the discharge, which is clearly seen in Fig. 4 (closed triangles). Visually, this nonuniformity looks like a bright core 10 cm in diameter around the axis.

As the field increased from 930 to 980 G, two effects were observed: first, a decrease in the average plasma density and, second, a rearrangement instability of the discharge resulting in a change in its shape. As the magnetic field approached 1000 G, the discharge became stable again, although variations in the plasma density attained 30% within the region 8 cm in diameter. As the magnetic field increased further, the plasma became even more uniform, whereas the central density remained almost unchanged. At $B_w > 1080$ G, radial variations in the ion current attained 3% within a region 160 mm in diameter (Fig. 4, squares). For a microwave power of $W = 900 \pm 30$ W and pressure of $p = 0.6$ mtorr, the current density and plasma density were equal to $J_i = 10$ mA/cm² and $N = 3.5 \times 10^{11}$ cm⁻³, respectively. We note that the high uniformity and high plasma density (exceeding the critical density by a fac-

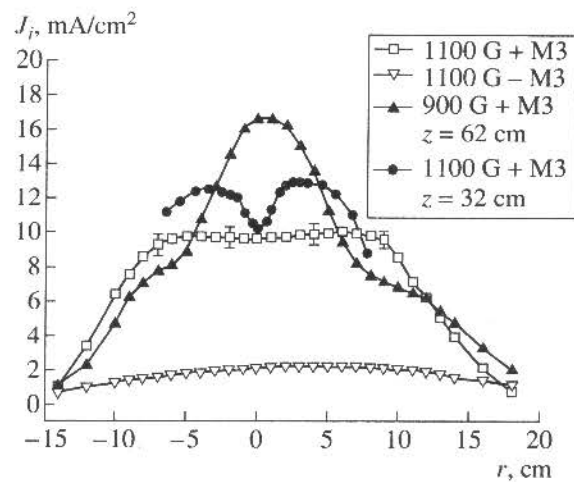


Fig. 4. Radial profiles of the ion saturation current density for different values of the magnetic field and different distances from the input window; Kr, $p = 0.6$ mtorr, the flow rate is 10 sccm, and $W = 900$ W; the magnetic field is produced by the electromagnets.

tor of 4.5) were observed at fairly large distances along the device axis: 62 cm from the input window and 49 cm from the middle of the ECR layer. Such a highly uniform and dense plasma was produced only if we switched on the third magnet mounted behind the plasmochemical reactor. Figure 4 also shows the radial profile of the ion current density when the third magnet is switched off (-M3). In this case, the current density, as well as the plasma density, is lower by a factor of more than 5 compared to the case when the third magnet is switched on and the radial homogeneity is much higher. Diffusion of electrons in a magnetized plasma occurs primarily along the magnetic field lines because of the large difference between the transverse and longitudinal mobilities; $b_{\perp}/b_{\parallel} \ll 1$. When the third magnet is switched off, the magnetic field produced by the other two magnets in the plasmochemical reactor is strongly converging. As a result, most of the particles produced in the source escape to the wall. The third magnet, together with the other two, creates a mirror magnetic field with a mirror ratio of $B_{\max}/B_{\min} \approx 3.7$ (Fig. 2) in the reactor. The plasma electrons are well confined in such a field, and the ions are confined via the ambipolar electric field. Therefore, the mirror configuration of the magnetic field in the plasmochemical reactor has a collimating effect and, thus, allows one to obtain a fairly high plasma density at large distances from the input window.

Figure 4 also shows the radial profile of the ion current density (circles) near the source throat (at a distance $z = 32$ cm from the input window). A specific feature of this profile is a hollow in the current density in the center of the discharge. Downstream the source, the hollow disappears due to radial diffusion.

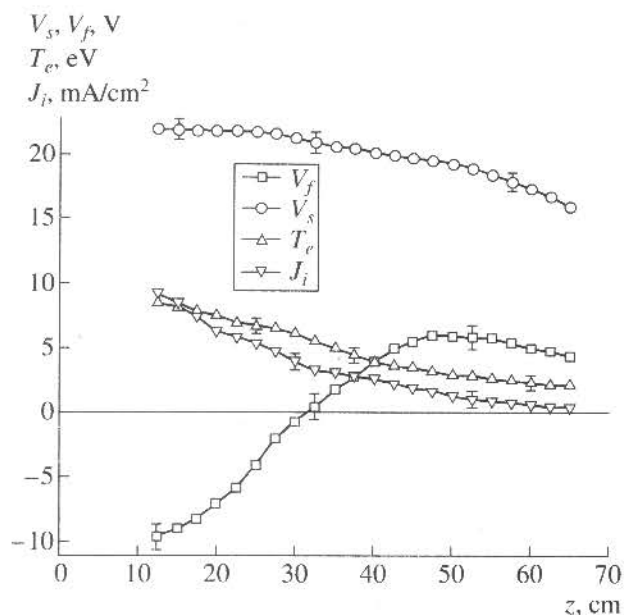


Fig. 5. Longitudinal profiles of the floating potential V_f , plasma potential V_s , electron temperature T_e , and ion current density J_i at $r = 0$: Ar, $p = 0.6$ mtorr, the flow rate is 8 sccm, $B_w = 1035$ G, and $W = 450$ W; the magnetic field is produced by the electromagnets M1 and M2.

Variations in the magnetic field in the device result in substantial variations in the magnitude and radial profile of the plasma density and the ratio between the incident and reflected powers (Fig. 3, closed triangles). When measuring these dependences, we did not refine the tuning of the triple-stub transformer. The maximum of the reflected power was observed when the resonance conditions were satisfied and an ECR layer was located on the inner surface of the microwave-input window, where the density gradient is fairly high. A high density gradient manifests itself as a jump in the spatial impedance, which results in an increase in the reflected power. As B_w increases, the resonant layer shifts from the window; as a result, the density gradient and, consequently, the reflected power decrease. At a magnetic field of 1010 G and higher, the ECR layer is located at a distance greater than 9 cm ($z_{ce} = 13$ cm for 1080 G). In this case, the reflected power is almost independent of the magnetic field and remains at a level of several percent. We note that the incident microwave is linearly polarized (i.e., it is a superposition of right- and left-polarized waves) and the electric field is maximum on the axis (TE_{11} mode in the source). The absorption of left-polarized waves and the formation of a dip in the plasma density profile for $N > N_{cr}$ were also observed in other similar devices [7, 8]. The suggested absorption mechanism is related to the conversion of these waves into plasma waves and the following Landau damping [7].

Figure 5 shows the longitudinal profiles of the main thermophysical plasma parameters, namely, the ion current density J_i , the electron temperature T_e , the plasma potential V_s , and the floating potential V_f . The profiles were obtained for the magnetic field produced by two electromagnets M1 and M2 only. It is seen that the ion current density (plasma density) at a distance of 62 cm from the microwave-input window decreases by a factor of 5 as compared to that at the source throat ($z = 25$ cm). In the absence of a third magnet, the density at $z = 47$ cm falls to the critical value, corresponding to the current density $J_i = 1.8$ mA/cm². As the distance increases, the electron temperature, which attains 10 eV near the ECR layer ($z = 12.5$ cm), decreases to 2 eV ($z = 65$ cm). The plasma potential V_s reaches its maximum (+22 V) in the ECR layer inside the source and decreases as z increases. The voltage between the source throat and the substrate region is 6 V. We note that this voltage does not exceed 2–3 V in a weakly converging field produced by three electromagnets. The floating potential V_f is minimum (–10 V) in the resonant region, where the concentration of high-energy electrons is fairly high. As the distance from the input window increases, the floating potential increases and then becomes positive.

3.2. Discharge in the Hybrid Magnetic Field

In this series of experiments, we investigated a plasma produced in a hybrid field, which is a superposition of a solenoidal field produced by two or three electromagnets and a cusp field produced by twelve permanent magnets positioned on the outer surface of the source. There are at least two reasons why we used permanent magnets: the use of these magnets reduces MHD plasma instabilities in the source and creates an additional ECR layer located near the source wall, thereby increasing the plasma density.

The ion current density as a function of the magnetic field and its radial profiles are shown in Figs. 3 and 6, respectively. The values of the magnetic field B_w produced by the electromagnets only (i.e., without the field produced by the permanent magnets) on the inner surface of the microwave-input window are also shown in the figures. The main features of the discharge in a hybrid magnetic field as compared with a solenoidal field can be formulated as follows.

(i) *Significantly better stability.* From a comparison of the dependences presented in Fig. 3, it is seen that the resonant peak is somewhat wider and has a flattened profile with a small dip in the center. For this reason, in discharges with a hybrid field, a plasma with a maximum density can be produced within a wider range of the magnetic field $900 \text{ G} \leq B_w \leq 940 \text{ G}$ and can be sustained for a longer time. Within the range $950 \text{ G} \leq B_w \leq 1100 \text{ G}$, in contrast to discharges with a solenoidal field, instabilities resulting in the rearrangement of the discharge are observed only at low pressures ($p \leq$

0.3 mtorr), whereas at higher pressures, the discharge is stable.

(ii) *Higher maximum plasma density.* For $B_w = 900$ G, $p = 0.6$ mtorr, and a microwave power of 900 W, the plasma density in the center of the discharge (at a distance of 62 cm from the microwave-input window) with a hybrid field is higher than that in a solenoidal field by a factor of about 1.5 (Fig. 3). The plasma densities at $z = 32$ cm ($N_i = 3 \times 10^{12}$ cm $^{-3}$) and $z = 62$ cm ($N_i = 10^{12}$ cm $^{-3}$) attain their maximum values at different pressures ($p = 1.5$ and 0.7 mtorr, respectively), which is explained by the collisions of ions with neutrals downstream the source. The degree of ionization of the working gas (Kr or Xe) attains 7% at the source throat.

(iii) *Substantially worse radial homogeneity of the discharge.* This is seen from a comparison of radial profiles in Figs. 4 and 6. In a hybrid field, radial variations in the plasma density are no less than $\pm 15\%$, whereas in a solenoidal field at $B_w = 1100$ G, they are as low as $\pm 2.5\%$ within a region 160 mm in diameter.

Figure 7 shows the radial profiles of the main thermophysical plasma parameters at the source throat ($z = 32$ cm). As is seen from the ion current profile, the discharge in this region has a shape of a core. The electron temperature is maximum in the center and is equal to 4–4.5 eV. As the distance from the discharge center increases, the temperature falls to 1.5 eV. In spite of a substantial plasma inhomogeneity, the plasma potential V_s varies only slightly in the radial direction. In the center of the discharge, the floating potential V_f is negative and the difference ($V_s - V_f$) is maximum and equal to 20 V. At the edge of the core, the floating potential is positive and the difference ($V_s - V_f$) is equal to 5–6 V. Such a high radial inhomogeneity of both the floating potential and the difference ($V_s - V_f$) is explained by the fact that the density of high-energy electrons increases substantially as the distance from the discharge center decreases. This is clearly seen in Fig. 8, which shows EEDF $f(E)$ for different distances from the core axis.

The EEDF is normalized as $\int_0^{E_{\max}} f(E) dE = 1$, where $E_{\max} = 35$ eV. The presence of a hot-electron population is the most pronounced near the axis (curve A, $r = 0.5$ cm), where the EEDF has two maximums. The maximum in the energy spectrum from 5 to 8 eV is associated with collisionless heating of electrons through their resonant interaction with microwaves. For comparison, in Fig. 8, the Maxwellian EEDFs,

$f(E) = \text{const} \sqrt{E} \exp\left(-\frac{3E}{2\bar{E}}\right)$ (gray curves), calculated for

the same values of the mean energy are also shown for $r = 6.5$ cm (curve E, the edge of the core) and $r = 0.5$ cm (curve A). It is seen that, even at the edge of the discharge, the EEDFs differ from Maxwellian, because the electron energy losses for ionization and excitation deplete the high-energy part of the EEDF as compared to the equilibrium EEDF.

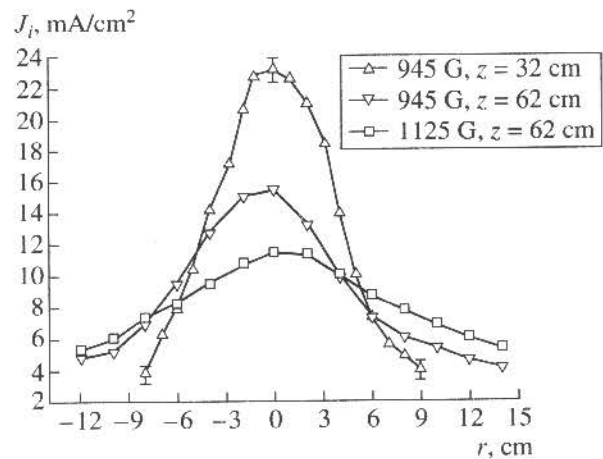


Fig. 6. Radial profiles of the ion current density in the hybrid magnetic field; Kr, $p = 0.5$ mtorr, the flow rate is 9 sccm, and $W = 600$ W.

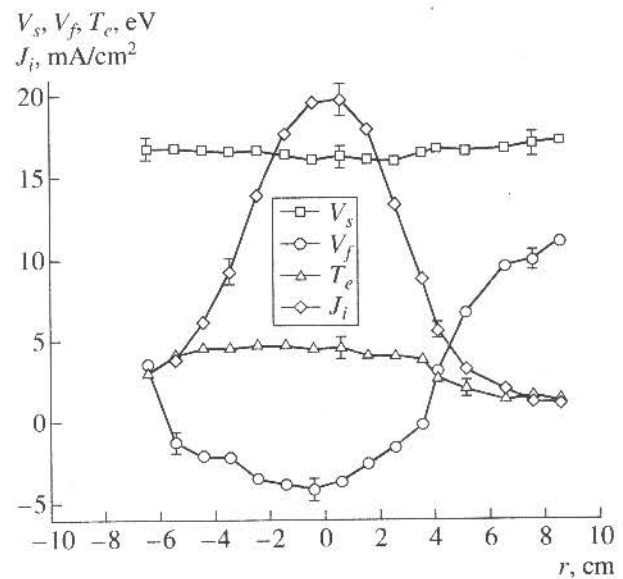


Fig. 7. Radial profiles of the floating potential V_f , plasma potential V_s , electron temperature T_e , and ion current density J_i near the source throat (at a distance of $z = 32$ cm from the microwave-input window) in the hybrid magnetic field; Kr, $p = 0.5$ mtorr, the flow rate is 9 sccm, $B_w = 945$ G, and $W = 600$ W.

3.3. Discharge in a Cusp Magnetic Field

In this series of experiments, the magnetic field was produced by the permanent magnets only, and the electromagnets, if any were used, produced a field substantially lower than the resonant field equal to 875 G.

The radial plasma density profiles at the distances $z = 32$ and 62 cm are shown in Fig. 9. The discharge plasma in the field produced by the permanent magnets has a low density on the order of several units of

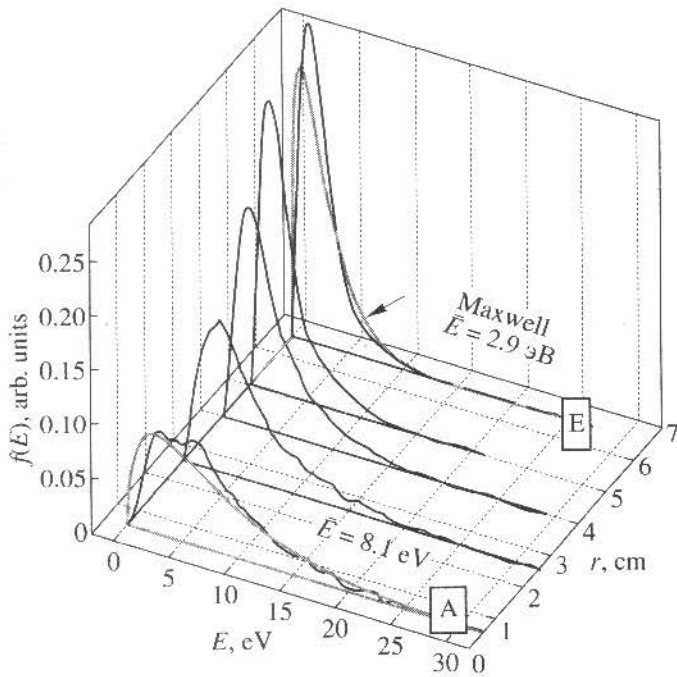


Fig. 8. Experimental (black curves) and Maxwellian (gray curves) EEDFs in the hybrid magnetic field at $z = 32$ cm and different radii; Kr, $p = 0.5$ mtorr, the flow rate is 9 sccm, and $W = 600$ W.

10^{-9} cm $^{-3}$ (triangles) because of the absence of optimal conditions for wave propagation in a cusp field (the magnetic field is close to zero for $r < 5$ cm). When the electromagnets are switched on to produce a low field ($B_w = 500$ G), the profile changes drastically (circles). The maximum density (on the order of $N_0 = N_{cr} = 7.4 \times$

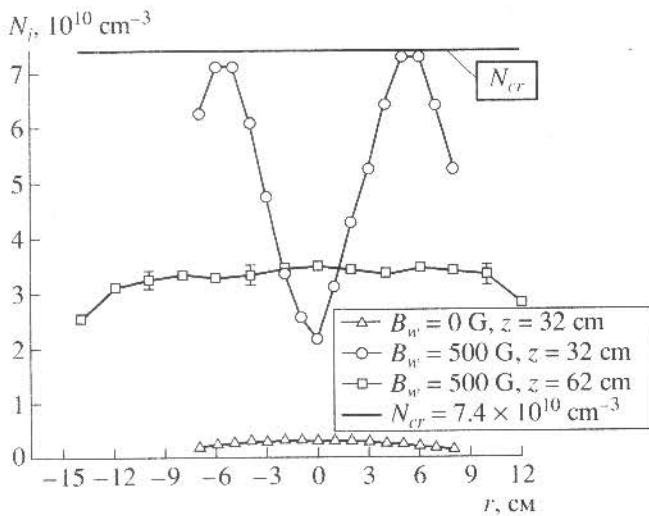


Fig. 9. Radial profiles of the plasma density in the cusp field produced by permanent magnets; Kr, $p = 0.5$ mtorr, the flow rate is 9 sccm, and $W = 760$ W.

10^{10} cm $^{-3}$) is observed at a distance of 5.5 cm from the device axis, and a dip appears in the center. Such a profile indicates that the absorption of microwaves occurs in an axisymmetric ring ~ 2 cm away from the source walls rather than on the chamber axis. In this case, the switching-on of the solenoidal field does not lead to the appearance of a new ECR layer but to a strong reduction in the radial diffusion and particle losses at the walls. The density profile at a distance of 62 cm from the microwave-input window in the case of a low solenoidal field (Fig. 9, squares) shows that, in a mirror magnetic field, even at a large distance from the source, the mean plasma density is only one-half as large as that in the cross section $z = 32$ cm. Furthermore, in this cross section variations in the plasma density are very low ($\pm 3\%$ within a region 200 mm in diameter).

Figure 10 shows the emission spectrum of Kr plasma at the source throat. The presence of intense ion lines shows a high degree of plasma ionization.

Figure 11 illustrates the instrumental function of a Fabry-Perot interferometer with a plate separation of 8 mm and the contour of the Kr $^{+}$ 4739 Å line measured at a distance of 62 cm from the input quartz window in the transverse direction to the magnetic field. The instrumental function is well fitted by the Lorentzian function. At such pressures, the Doppler effect makes the main contribution to the broadening of emission contours of atoms and ions (a polaroid prevented Zeeman broadening). In this case, the full contour is described by the Voigt function, which is a Gaussian profile convoluted with a Lorentzian one. The reduction procedure allowed us to determine the Gaussian component and calculate from it the temperature of heavy particles. The temperatures of atoms and ions (Ar, Kr, Xe) were found to be no higher than 0.1 and 0.4 eV,

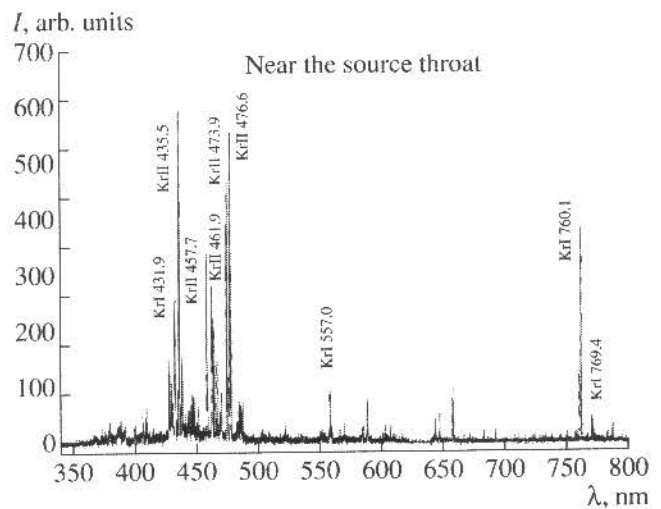


Fig. 10. Spectrum of Kr plasma emission near the source throat for; $p = 0.5$ mtorr, the flow rate is 9 sccm, and $W = 600$ W.

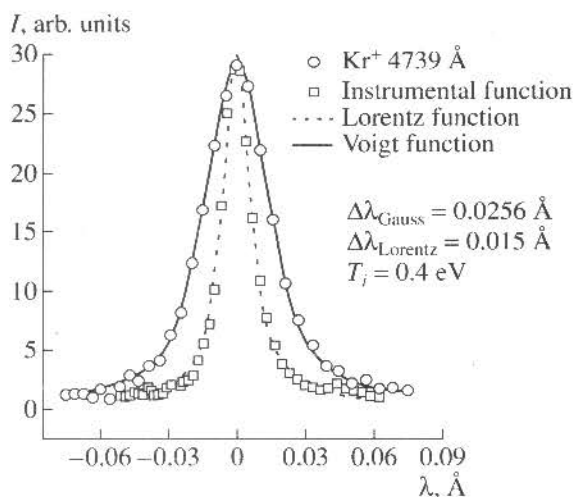


Fig. 11. Contours of spectral lines: the instrumental function (squares) of the Fabry–Perot interferometer ($t = 8$ mm, $\lambda = 6328$ Å) and its Lorentzian fit (dashed line) and the profile of the Kr^+ 4739 Å line (circles) and its Voigt-function fit (solid line); $p = 0.6$ mtorr, the flow rate is 10 sccm, B_{H} = 950 G, and $W = 800$ W.

respectively, within a pressure range of 0.4–1 mtorr. The energy of directed motion of ions arriving at an insulated substrate, $V_p - V_f$, lies in the interval 15–35 eV. Such a relationship between the energies of thermal and directed motion permits anisotropic etching of submicron structures with high aspect ratios [9].

4. CONCLUSION

The influence of the magnetic-field configuration on the plasma parameters in a microwave ECR discharge

has been studied. The conditions necessary for obtaining high plasma homogeneity and/or high plasma density are found. The experiments show that, by varying the magnetic-field configuration, it is possible to obtain plasma parameters required for various plasma technologies used in the production of microelectronic components.

ACKNOWLEDGMENTS

This work was supported by the Ministry of Education of the Russian Federation under the program “Critical Technologies.”

REFERENCES

1. Asmussen, J., *J. Vac. Sci. Technol. A*, 1989, vol. 7, no. 3, p. 883.
2. Maeda, M. and Ameniya, H., *Jpn. J. Appl. Phys.*, 1994, vol. 33, p. 5032.
3. Shibuki, S., Kanao, H., and Akahori, T., *J. Vac. Sci. Technol. B*, 1997, vol. 15, p. 60.
4. Poluektov, N.P. and Tsar’gorodtsev, Yu.P., *Prib. Tekh. Eksp.*, 1996, no. 4, p. 150 [*Instrum. Exper. Tech.* (Engl. transl.), 1996, vol. 39, p. 611].
5. Steinbruchel, C., *J. Vac. Sci. Technol. A*, 1990, vol. 8, p. 1663.
6. Ginzburg, V.L., *The Propagation of Electromagnetic Waves in Plasmas*, Oxford: Pergamon, 1970.
7. Popov, O.A., *J. Vac. Sci. Technol. A*, 1991, vol. 9, no. 3, p. 711.
8. Gorbatkin, S.M., Berry, L.A., and Roberto, J.B., *J. Vac. Sci. Technol. A*, 1990, vol. 8, p. 2893.
9. Ogino, S., Fujiwara, N., Maruyama, T., *et al.*, *Jpn. J. Appl. Phys.*, 1997, vol. 36, p. 2491.

Translated by N. F. Larionova